Advanced Quenching Techniques for Super-Regenerative Radio Receivers

Félix Omar Fernández-Rodríguez, *Student Member, IEEE*, and Edgar Sánchez-Sinencio, *Life Fellow, IEEE*

***Abstract*—This paper proposes an optimal super-regenerative-receiver quench signal that achieves 48% narrower 3 dB bandwidth than state of the art and in addition allows independent selection of receiver gain, 3 dB bandwidth, and maximum quench frequency, facilitating design. While many previous works have focused on building block-level optimization, we present a circuit-independent, system-level optimization of the quench signal and demonstrate that key receiver performance is intricately tied to this wave shape. This work both theoretically derives how to optimize the quench signal and experimentally verifies the predicted performance improvement with a discrete-element prototype. Measured results show over 42% reduction in 3 dB bandwidth by optimally changing the quench-signal shape for a given gain and quench frequency.**

***Index Terms*—Low power receivers, super-regenerative receivers.**

I. Introduction

THE super-regenerative receiver (SRR) dates back to Edwin Armstrong's early 1920s patents [1], [2]. At that time the simplicity of using a single active element—then a vacuum tube—to achieve significant gains at radio frequencies was groundbreaking. The super-regenerative receiver achieves these gains by exploiting the ability of an unstable system to achieve exponentially growing oscillation when the proper conditions are present. These oscillations are controlled by a time-varying signal known as the quench signal. The downside of the super-regenerative receiver is wide 3 dB bandwidth (BW). When Armstrong developed the heterodyne receiver [3], capable of far superior selectivity, the super-regenerative receiver technique faded into obscurity—that is, until recently [4]–[16].

Super-regenerative receivers present several characteristics that make them attractive for recent applications, mainly low power [4]–[11] and super high frequency (SHF) [12]–[14] to extremely high frequency (EHF) [17] receivers. The simplicity of the super-regenerative receiver and intermittent operation makes it possible to design a receiver consuming nJ/bit during reception. The small number of active devices allows for low complexity designs which are ideal for SHF and EHF designs. Moreover, these inherent characteristics do not depend on technology.

As mentioned above, SRRs also present several potential disadvantages, such as wide 3 dB BW. As we shall show, the proper quench-signal shape mitigates this 3 dB BW concern.

Recent designs [5]–[7], [10], [11] have focused on optimizing the system's building blocks and basically operate the receiver in the same manner as the original works did, except for [6], where frequency tuning was included, and [11] where a piecewise linear quench signal was implemented to achieve narrower 3 dB BW. Although a good step forward, these publications did not exploit the maximum potential of the super-regenerative receiver. The piecewise quench signal opens the door for independent control over the receiver's gain, selectivity, and data rate.

The main contribution of this work is the optimal quench-signal design and hardware verification of that signal's 3 dB BW reduction capability. The basic theory behind the super-regenerative receiver is discussed in Section II. This section emphasizes how apparent SRR limitations can be circumvented with appropriate quench-signal design. Section III derives the desired quench signal based on the previous theoretical discussion. A theoretical comparison between several quench signal shapes including classical waveforms and recently proposed waveforms is presented in Section IV. Next, Section V presents an experimental hardware prototype to demonstrate the optimal quench signal in hardware and to compare to conventional waveforms. Finally, Section VI concludes the paper.

II. Super-Regenerative Theory

This section summarizes the necessary SRR theory to understand the implications of proper quench-signal design; for more detailed theory, see [18]–[23]. At the heart of every super-regenerative receiver, and regenerative amplifier for that matter, is a selective network with a controlled positive feedback network. This network may be modeled as a parallel LC tank with a negative conductance representing the positive feedback. We denote this network as a super-regenerative oscillator (SRO).

In SROs the main interest is the intermittent growth and decay of oscillations, i.e., oscillator startup, due to the positive feedback, i.e., negative conductance—not the steady state response. These oscillations are not only due to general noise but more importantly the possible AC signal applied at the input. This input signal is modeled as an AC current source applied to the LC tank. Fig. 1 shows the basic schematic of the SRO network where G_o is the system's nominal conductance and $K(t) \cdot g_m$ is a (time-varying) negative transconductance. In the

Manuscript received May 09, 2011; revised September 05, 2011; accepted October 17, 2011. Date of publication January 16, 2012; date of current version June 22, 2012. This work was supported in part by Texas Instruments. This paper was recommmended by Associate Editor A. Tasic.

The authors are with Analog and Mixed Signal Center, Texas A&M University, College Station, TX 77843 USA (email: felixf@tamu.edu; sanchez@ece.tamu.edu).

Digital Object Identifier 10.1109/TCSI.2011.2177010

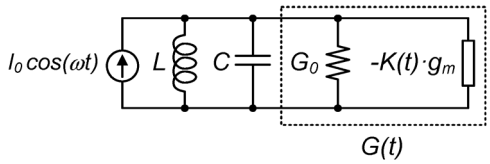

Fig. 1. Super-regenerative oscillator model: LC tank and time-varying negative conductance.

following discussion, we initially assume $K(t)$ is a constant (K) for simplicity.

The differential equations that describe the voltage across the tuned tank are

$$C\frac{dv(t)}{dt}+(G_o-K\cdot g_m)v(t)+\frac{1}{L}\int v(t)dt=I_0\cos(\omega t) \quad (1)$$

$$C\frac{d^2v(t)}{dt^2}+(G_o-K\cdot g_m)\frac{dv(t)}{dt}+\frac{v(t)}{L}=-I_0\omega\sin(\omega t). \quad (2)$$

The solution for the equation of voltage across the tank when $v(0)=0$, $I_0\cos(\omega t)=0$, $v'(0)=0$, and $\omega=\omega_o$ is

$$v(t)=\frac{I_0}{G_o-K\cdot g_m}\frac{\omega_o}{\omega_d}\exp\left(-\frac{G_o-K\cdot g_m}{2C}t\right)\times\sin(\omega_d t)+\frac{I_0\sin(\omega_o t)}{G_o-K\cdot g_m} \quad (3)$$

where $\omega_d=\sqrt{\omega_o^2-\alpha^2}$ is the frequency of the damped oscillation, $\alpha=(G_o-K\cdot g_m)/2C$, and $\omega_o=1/\sqrt{LC}$ is the natural frequency of the tuned circuit. The first term in (3) is the most important and represents the transient component. If $G_o-K\cdot g_m$ is fixed to a constant negative value, the first term grows exponentially, while if $G_o-K\cdot g_m$ is fixed to a constant positive value, the first term decays to zero. The dynamics of the amplitude growth of these oscillations depend on the amplitude of the applied signal. The oscillation frequency depends on the amount of feedback (i.e., negative conductance) applied.

n an SRO the value of the overall conductance is made to alternate from positive to negative values, which allows oscillations to grow or decay. The overall conductance may be varied by two fundamental methods. First, the negative conductance may be increased by increasing the amount of feedback. Second, the overall conductance may be increased by adding extra damping conductance to the system.

A. Linear-Mode Operation

When the transient oscillation waveforms exponentially grow but are subsequently damped before reaching their maximum steady-state value, the SRO is said to operate in linear-mode. This term arises from the linear relationship between the maximum amplitude reached by the oscillations and the amplitude of the applied signal.

For the linear-mode analysis, let the system conductance be a general function of time $G(t)=G_o-K(t)\cdot g_m$. This time-varying conductance function is commonly generated by an SRO signal called the *quench signal*, as it quenches the oscillation when it attains a positive conductance value, and it allows for oscillations buildup when it becomes a negative conductance value. In this paper we assume a one-to-one relationship between the quench signal and the conductance signal; for example if the quench signal were the gate voltage

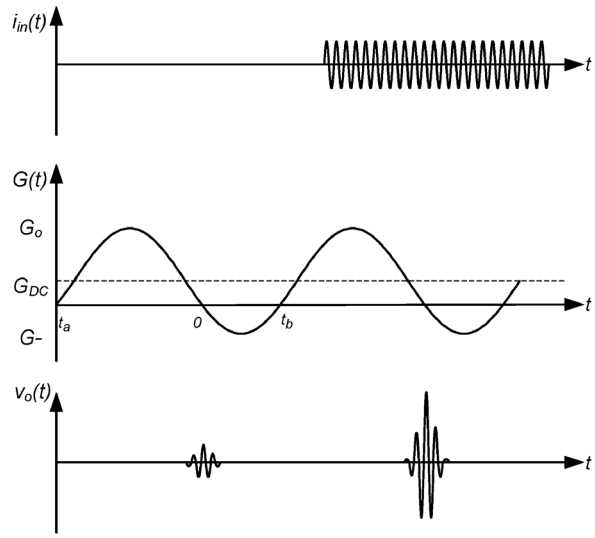

Fig. 2. SRO's current input signal, time-varying conductance function, and output voltage.

$V_{g,\mathrm{quench}}(t)$ of a triode-region NFET, then the conductance signal would be: $G(t)\equiv\mu_n C_{OX}(W/L)(V_{g,\mathrm{quench}}(t)-V_T)$. A sinusoidal-conductance example waveform is shown in Fig. 2 along with the SRO's input current and output voltage.

$$\frac{d^2v(t)}{dt^2}+\frac{G(t)}{C}\frac{dv(t)}{dt}+\left(\omega_o^2+\frac{1}{C}\frac{dG(t)}{dt}\right)v(t)=-\frac{I_0\omega}{C}\sin(\omega t). \quad (4)$$

Replacing the term $dv(t)/dt$ from the previous by changing the variable $v(t)$ to

$$v(t)=y(t)\exp\left(-\frac{1}{2C}\int_{t_a}^{t}G(x)dx\right) \quad (5)$$

in (4) yields

$$\frac{d^2y(t)}{dt^2}+\left(\omega_o^2+\frac{1}{2C}\frac{dG(t)}{dt}-\frac{G(t)^2}{4C^2}\right)y(t)=-\frac{I_0\omega}{C}\sin(\omega t)\exp\left(\frac{1}{2C}\int_{t_a}^{t}G(x)dx\right). \quad (6)$$

We now solve for $y(t)$ by making the following assumption:

$$\omega_o^2\gg\left|\frac{1}{2C}\frac{dG(t)}{dt}-\frac{G(t)^2}{4C^2}\right| \quad (7)$$

which reduces (6) to

$$\frac{d^2y(t)}{dt^2}+\omega_o^2y(t)\approx-\frac{I_0\omega}{C}\sin(\omega t)\exp\left(\frac{1}{2C}\int_{t_a}^{t}G(x)dx\right). \quad (8)$$

This equation is a second-order, nonhomogeneous, linear ordinary differential equation (ODE) with constant coefficients; for which the solution is given by two components: the general solution and the particular solution [24].

The general or homogeneous solution yields

$$\frac{d^2y(t)}{dt^2}+\omega_o^2y(t)=0 \quad (9)$$

$$y_g(t)=C_1\sin(\omega_o t)+C_2\cos(\omega_o t), \quad (10)$$

clearly a constant oscillation function which is of no interest in the super-regenerative behavior.

Using the variation of parameters technique [24], as previously shown in [18], [21], the particular solution is given as

$$y_p(t) = -\frac{I_0\omega}{C}\frac{1}{\omega_o} \times \left\{ \sin(\omega_o t) \int_{t_a}^{t} \cos(\omega_o \tau)\sin(\omega\tau) \times \exp\left(\frac{1}{2C}\int_{t_a}^{\tau} G(x)dx\right) d\tau - \cos(\omega_o t) \int_{t_a}^{t} \sin(\omega_o\tau)\sin(\omega\tau) \times \exp\left(\frac{1}{2C}\int_{t_a}^{\tau} G(x)dx\right) d\tau \right\} \quad (11)$$

after some trigonometric manipulations the particular solution is simplified to

$$y_p(t) = -\frac{I_0\omega}{C\omega_o} \int_{t_a}^{t} \exp\left(\frac{1}{2C}\int_{t_a}^{\tau} G(x)dx\right) \times \sin(\omega\tau)\sin\left(\omega_o(t-\tau)\right) d\tau. \quad (12)$$

Substituting into (5) yields

$$v_p(t) = -\frac{I_0\omega}{C\omega_o} \exp\left(-\frac{1}{2C}\int_{t_a}^{t} G(x)dx\right) \times \int_{t_a}^{t} \exp\left(\frac{1}{2C}\int_{t_a}^{\tau} G(x)dx\right) \sin(\omega\tau)\sin\left(\omega_o(t-\tau)\right) d\tau. \quad (13)$$

This growing or decaying voltage is the key point of interest in the study of super-regenerative receivers. These common expressions typically ease manipulation of the particular solution [18], [21]:

$$K_s = \exp\left(-\frac{1}{2C}\int_{0}^{t_b} G(x)dx\right) \quad (14)$$

$$s(t) = \exp\left(\frac{1}{2C}\int_{0}^{t} G(x)dx\right) \quad (15)$$

$$p(t) = \exp\left(-\frac{1}{2C}\int_{t_b}^{t} G(x)dx\right) \quad (16)$$

where K_s is the *super-regenerative gain*. The super-regenerative gain is due to the oscillation build-up during the negative portion of the conductance within the quench period, and its value is determined by the area enclosed by the conductance curve during this time period (e.g., area $A-$ in Fig. 3). The *sensitivity* pulse $s(t)$ is a weighting function of the incoming signal; it reaches it maximum value in the vicinity of the conductance transition from positive to negative value (i.e., the *sensitivity period*). This weighting function implies that the SRR can be seen as a RF bandpass sampling system (as described later) with sampling period given by $s(t)$. Finally, $p(t)$ is the normalized oscillation-envelope shape observed at the output node. Fig. 3 shows a typical quench signal with a sinusoidal shape. Though suboptimal, this shape is easy to implement and hence commonly used. With these substitutions the particular solution can be expressed as

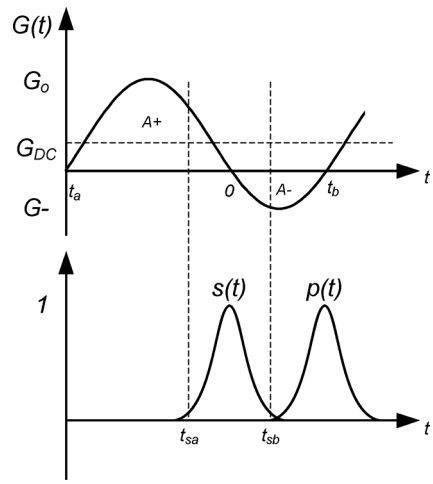

Fig. 3. Typical sine wave conductance quench signal $G(t)$, equivalent normalized sensitivity pulse $s(t)$ and normalized output envelope $p(t)$.

$$v_p(t) = -K_s p(t)\frac{I_0\omega}{C\omega_o} \int_{t_a}^{t} s(\tau)\sin(\omega\tau)\sin\left(\omega_o(t-\tau)\right) d\tau. \quad (17)$$

The above expression can be shown to have two cosine function terms at $\omega_o \pm \omega$. When these frequencies are close to each other, as they typically are in receiver applications, the additive terms oscillate so fast that the integration action averages then to nearly zero. Thus, the particular solution is approximately

$$v_p(t) \approx K_s p(t)\frac{I_0\omega}{2C\omega_o} \int_{t_a}^{t} s(\tau)\cos\left(\omega_o t + \tau(\omega-\omega_o)\right) d\tau. \quad (18)$$

The integration limits may be constrained to (t_{sa}, t_{sb}), defined by the sensitivity period, as shown in Fig. 3, because $s(t)$ is very small outside these limits. For the same reason, we can replace the sensitivity-period integration limits with $\pm\infty$. Finally, using the exponential notation

$$v_p(t) \approx K_s p(t)\frac{I_0\omega}{2C\omega_o} \times \Re\left[\int_{-\infty}^{+\infty} s(\tau)\exp\left(-j(\omega_o-\omega)\tau\right) d\tau \exp(j\omega_o t)\right] \quad (19)$$

where $\Re[]$ denotes the real part of the complex number notation. The integral term is a frequency shifted Fourier transform of the

sensitivity pulse. Including this fact, the particular solution may be rewritten as

$$v_p(t) \approx K_s p(t) \frac{I_0 \omega}{2C\omega_o} \Re\left[\mathcal{S}(\omega_o - \omega)\exp(j\omega_o t)\right] \tag{20}$$

where $\mathcal{S}(\omega_o - \omega) = \mathcal{F}\{s(\tau)\exp(-j(\omega_o - \omega))\tau\}$, is the previously mentioned Fourier transform. Finally, we introduce the *regenerative gain* K_r

$$K_r = \frac{G_o}{2C}\int_{t_{sa}}^{t_{sb}} s(t)dt = \frac{G_o}{2C}\mathcal{S}(0). \tag{21}$$

Using this notation the particular solution is now expressed as

$$V_p(t) \approx K_r K_s p(t) \times \frac{I_0}{G_o}\underbrace{\frac{\omega}{\omega_o}\frac{|\mathcal{S}(\omega_o-\omega)|}{\mathcal{S}(0)}}_{|H(\omega)|}\cos\left(\omega_o t + \angle\mathcal{S}(\omega_o-\omega)\right) \tag{22}$$

$$V_p(t) \approx K_r K_s p(t)\frac{I_0}{G_o}|H(\omega)|\cos\left(\omega_o t + \angle\mathcal{S}(\omega_o-\omega)\right) \tag{23}$$

where $|H(\omega)|$ is a bandpass function centered around ω_o. This bandpass function sets the frequency response of the super-regenerative receiver.

The implications of assumption (7) are now considered. Rewriting the assumption in terms of $Q_o = (\omega_o C)/G_o$ and letting the maximum value of $G(t)$ be G_o, we have

$$\omega_o^2 \gg \left|\frac{1}{2C}\frac{dG(t)}{dt} - \frac{\omega_o^2}{4Q_o^2}\right|. \tag{24}$$

The second term on the right hand side may be ignored for reasonable values of Q_o, so

$$\omega_o^2 \gg \left|\frac{1}{2C}\frac{dG(t)}{dt}\right| \tag{25}$$

$$\frac{dG(t)}{dt} \ll 2\omega_o G_o Q_o \tag{26}$$

this implies that the rate of change of conductance must be small compared to the oscillation frequency of the tuned system for the previous derivation to hold true. Next, we consider the two extremes of conductance transition during the quench period. The first is a gradual transition or slope-controlled conductance. The other is a sharp transition or step-controlled conductance.

1) Slope-Controlled Conductance: In sloped-controlled systems the conductance changes linearly. Fig. 4 shows an example of a slope-controlled conductance curve. The conductance function can be defined as

$$G(t) = \left(\frac{G_- - G_0}{t_b - t_a}\right)t = G' \cdot t \tag{27}$$

where $G' < 0$ and assuming a constant slope throughout the whole quench period. The sensitivity pulse is hence

$$s_{\text{slope}}(t) = \exp\left(\frac{1}{2C}\int_0^t G' \cdot \tau d\tau\right) = \exp\left(\frac{1}{4C}G' \cdot t^2\right). \tag{28}$$

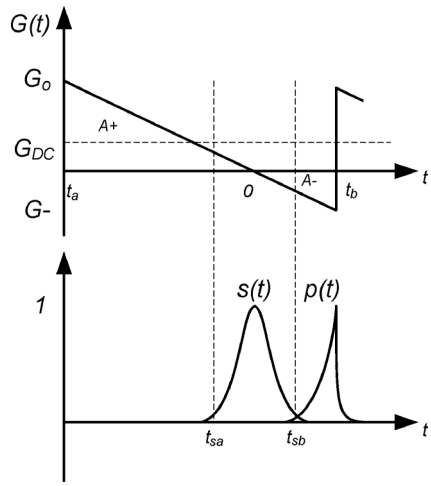

Fig. 4. Conductance curve for the slope-controlled quench signal $G(t)$, equivalent normalized sensitivity pulse $s(t)$ and normalized output envelope $p(t)$.

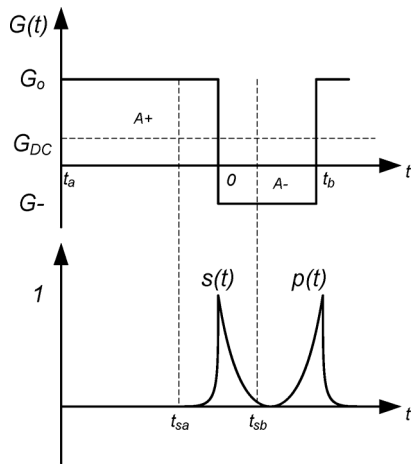

Fig. 5. Conductance curve for the step-controlled quench signal $G(t)$, equivalent normalized sensitivity pulse $s(t)$ and normalized output envelope $p(t)$.

Taking its Fourier transform, we obtain

$$\mathcal{F}\left\{s_{\text{slope}}(t)\right\} = \mathcal{S}(\omega) = \sqrt{\pi\frac{4C}{G'}}\exp\left(-\frac{C\omega^2}{G'}\right) \tag{29}$$

so the frequency response is

$$H(\omega) = \frac{\omega}{\omega_o}\exp\left(-\frac{C(\omega_o-\omega)^2}{|G'|}\right). \tag{30}$$

From the previous discussion, we hence conclude that reducing the conductance slope $G' = dG(t)/dt$ reduces the 3 dB BW.

2) Step-Controlled Conductance: Conductance during the step-controlled case changes abruptly as shown in Fig. 5. This sharp transition violates the assumption given in (7), and the system must be reconsidered [18]. For the step-controlled systems the conductance function can be expressed as

$$G_{\text{step}}(t) = \begin{cases} G_0 u(-t) & t < 0 \\ G_- u(t) & t > 0 \end{cases} \tag{31}$$

where $G_0 > 0, G_- < 0$, and $u(t)$ is the Heaviside step function. The sensitivity pulse is

$$s_{\text{step}}(t) = \begin{cases} \exp\left(\frac{G_0}{2C}t\right) u(-t) & t < 0 \\ \exp\left(\frac{-|G_-|}{2C}t\right) u(t) & t > 0 \end{cases}. \tag{32}$$

The Fourier transform of the sensitivity function is

$$\mathcal{F}\{s_{\text{step}}(t)\} = \frac{1}{\left(-\frac{G_0}{2C}\right) - j\omega} + \frac{1}{\left(\frac{|G_-|}{2C}\right) + j\omega} \tag{33}$$

hence, the frequency response is

$$|H(\omega)|^2 = \left(\frac{\omega}{\omega_o}\right)^2 \frac{1}{\left[1 + \left(\frac{\omega_o - \omega}{G_0/2C}\right)^2\right]\left[1 + \left(\frac{\omega_o - \omega}{|G_-|/2C}\right)^2\right]} \tag{34}$$

which corresponds to a band-pass filter with second-order low-pass-equivalent response, so the Q is improved by reducing either $|G-|$ or G_0.

B. Self-Quenched Operation

There is one last type of SRR in which the quench signal is controlled by the super-regenerative circuit itself; these are known as self-quenching super-regenerative receivers. The behavior of such receivers mimics that of a squegging oscillator [18], [25]. The main difference from a typical implementation is the lack of an external quench-signal generator.

The self-quenched receiver's oscillations, as in the externally quenched ones, build up from the voltage present in the LC tank. Unlike the externally quenched receivers, the self-quenched receivers quench the growing oscillations once it reaches a desired voltage (V_{EQ}); the cycle then repeats. Fig. 6 presents quench cycles for self-quenching receivers when there is an incoming signal (dashed gray lines) and when oscillations build up form noise (solid black lines). Based on this figure one can see that when incoming signals are present in the tank; the pulse rate (number of pulses per unit time) increases relative to that of pulses starting from noise (i.e., $t_2 < t_1$). This difference in quench frequency will indicate whether or not the desired signal is present. We use a simple model to determine this difference in time, which we will call Δt. The simplified model assumes the buildup curves to be truly exponential until V_{EQ} is reached. This simplified model is quite accurate in practice [18], [26]. The build-up envelopes can be expressed as

$$V_{EQ} = V_1 \exp\left(\frac{t_1}{\tau_{LC}}\right) = V_2 \exp\left(\frac{t_2}{\tau_{LC}}\right) \tag{35}$$

$$V_1 = \sqrt{\overline{V_n^2}} K_{eq} \tag{36}$$

$$V_2 = \sqrt{\overline{V_n^2} + V_s^2} K_{eq} \tag{37}$$

where $\overline{V_n^2}$ is the mean square noise at the input, V_s is the signal voltage at the input, K_{eq} is the effective gain and frequency response of the receiver up to the time where the voltages reach

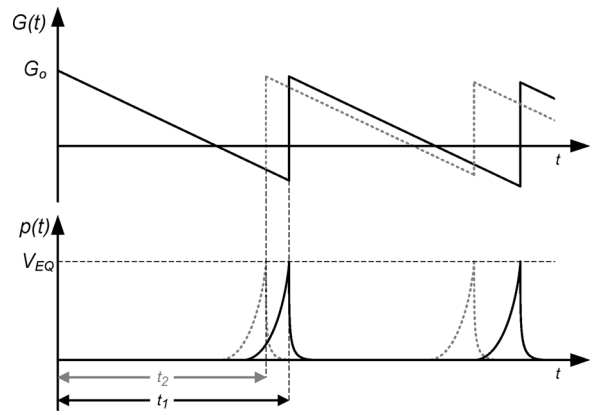

Fig. 6. Quench cycles for self-quenching receivers when there is an incoming signal (dasehed gray lines) and when oscillations build up form noise (solid black lines).

V_{EQ}, and τ_{LC} is the time-constant of build-up. The time it takes the oscillation to build up to V_{EQ} is

$$t_1 = \tau_{LC} \ln \frac{V_{EQ}}{V_1} \tag{38}$$

$$t_2 = \tau_{LC} \ln \frac{V_{EQ}}{V_2}. \tag{39}$$

Finally the time difference is

$$\begin{aligned} \Delta t = t_1 - t_2 &= \tau_{LC}\left[\ln \frac{V_{EQ}}{V_1} - \ln \frac{V_{EQ}}{V_2}\right] \\ &= \tau_{LC} \ln\left(\frac{V_2}{V_1}\right) \\ &= \tau_{LC} \ln\left(\sqrt{1 + \frac{V_s^2}{V_n^2}}\right). \end{aligned} \tag{40}$$

Based on (40) the signal detection of self-quenching SRRs operates in a logarithmic fashion (i.e., *logarithmic-mode*). Logarithmic-mode SRRs are know to have wider 3 dB BW [18]. During this discussion we will focus on linear-mode operation SRRs.

From all the previous discussion it is clear that the SRR performance is tightly coupled to the time-varying conductance shape. As previously mentioned this conductance is termed as the quench signal. The main goal is to obtain a quench signal which can exploit the main characteristics of SRRs (simplicity, low power consumption, and large RF gains) and mitigate the SRR's shortcomings (e.g., 3 dB BW) independent of circuit implementation.

III. Optimal Quench Signal

The shape of the quench signal dictates the gain, frequency response, and maximum data-rate, which are the principal specs (discussed in further detail in following subsections). Other system specifications such as selectivity, out-out-band interference, and minimum detectable signal (i.e., sensitivity)

fall out of the scope of our discussion. An "optimal" quench signal would achieve gain, frequency response, and high-data rate simultaneously. Note that the quench frequency determines the maximum data rate (explained below).

A. Gain

Two main factors determine the overall receiver gain: super-regenerative gain K_s and regenerative gain K_r

$$K_s = \exp\left(-\frac{1}{2C}\int_0^{t_b} G(x)dx\right) \tag{41}$$

$$K_r = \frac{G_o}{2C}\int_{t_{sa}}^{t_{sb}} s(\tau)d\tau = \frac{G_o}{2C}\int_{t_{sa}}^{t_{sb}} \exp\left(\frac{1}{2C}\int_{t_{sb}}^{t_{sb}} G(x)dx\right)d\tau. \tag{42}$$

The first is an exponential version of the area labeled A^- in Fig. 3. The second is the area contained by the sensitivity pulse, which is typically only a small portion of the overall quench period. From this information, we conclude that $K_s \ll K_r$ and that to maximize the overall gain, the area A^- must be maximized.

B. Frequency Response

The system's frequency response (i.e., its 3 dB BW) is given by (30) for the slope-controlled system and by (34) for the step-controlled one. To decrease the 3 dB BW of the slope-controlled systems the rate of change of the conductance function needs to be minimized. Minimizing this slope should be done independently of any other parameter. On the other hand, for the step-controlled system both the maximum and minimum conductance magnitudes should be reduced. Ideally, the maximum and minimum should both be tuned independently of other parameters.

C. Quench Frequency

The Nyquist criterion limits the lowest quench frequency to twice the signal bandwidth [27]. The upper limit of the quench frequency is set by the assumption that a quench period is influenced only by the incoming signal and not by remaining oscillations from a previous cycle. Until now this assumption was taken for granted.

The case where remaining oscillations from previous quench periods affect the current ones is termed the *hangover state*. The *hangover coefficient* defines the ratio between the current cycle's oscillation amplitude and the next's. This hangover coefficient [21] is

$$h = \exp\left(-\frac{G_{\rm dc}}{2Cf_q}\right) \tag{43}$$

where $G_{\rm dc}$ is the average or dc conductance value, and f_q is the *quench frequency* (i.e., $1/f_q = T_q = t_b - t_a$). From the previous discussion, a maximum quench frequency for a desired hangover coefficient is

$$f_q \le \frac{G_{\rm dc}}{2C}\frac{1}{\ln(1/h)} \tag{44}$$

Clearly, the maximum frequency is not limited by the conductance function's shape but by its average or dc value.

In practical, noncoherent SRR implementations, the quench signal samples the incoming bit period several times. The number of quench periods within a data bit depends on the desired modulation and bit-error-rate (BER), and thus must be considered on a case-by-case basis. The desired information in that case is the average envelope of the generated RF pulses. The frequency relationship is $f_b \ll f_q \ll f_0$, where f_b is the bit rate. This oversampling rate limits the maximum data rate. If the quenching signal were perfectly synchronized to the incoming bit sequence then $f_b \approx f_q$, increasing the attainable data rate. The synchronization scheme is still an open research problem.

D. Recently Published SRRs and Their Quench Signals

Recently, low-power applications have sparked renewed interest in the super-regenerative architecture. Next, we discuss the pros/cons of recently published approaches.

1) Sawtooth: In [10] the quench signal provides a slope-controlled system based on a conductance signal that may be approximated by the sawtooth curve in Fig. 4. K_s is limited by the triangular shape of the $A-$ area, reducing the overall system gain. The adjustable slope presented in [10] allows for different choices of system's 3 dB BW for different applications, but in reducing the slope, the super-regenerative gain K_s also reduces.

2) Square: [7] quenches the oscillations by switching on a small shunt resistance (large conductance) in parallel with a high-Q BAW resonator. Fig. 7 presents the conductance curve. The system's inherent small-magnitude conductance during the regenerative state forces a low quench frequency to allow a high enough K_s. A resistive element may be used to de-Q the system, and better balance may be achieved between the $A+/A-$ ratio. This will in turn increase K_s and allow for a higher quench frequency. However, reducing the Q also increases 3 dB BW and increases the power consumption.

3) Piecewise Linear: [8] implements a piecewise-linear conductance function. Fig. 8 illustrates a simplified version of this function. First, the piecewise-linear function assumes a constant, large conductance value for a short period of time ($\approx T_q/10$) with the intent to quench any previous oscillations. Next, the conductance drops to to an extremely low value, termed *critical conductance* for $t \in [T_q/10, T_q/2]$, corresponding to a high-Q filter as discussed in Section II-A2. This critical conductance is so named because it biases the SRO at the verge of oscillation—e.g., in [8], the piecewise linear signal was implemented by a 9-bit DAC, which placed the critical conductance (*critical current* in [8]) 1LSB above the oscillation condition. Finally, the curve features a ramp with controlled slope for the remaining $T_q/2$ of the interval.

This quench signal provides several advantages over more conventional ones. The time period $t_r \to 0$ effectively widens the sensitivity pulse, thereby increasing K_r. Furthermore, as in

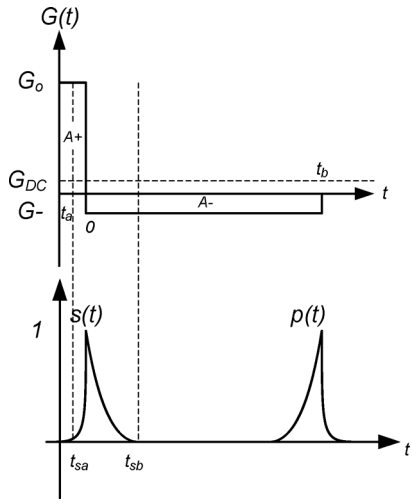

Fig. 7. [7] conductance curve $G(t)$, equivalent normalized sensitivity pulse $s(t)$ and normalized output envelope $p(t)$.

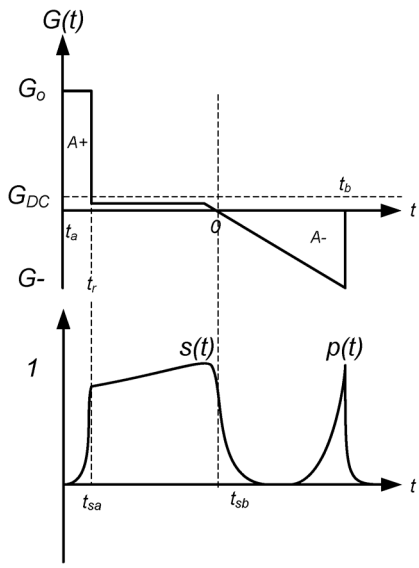

Fig. 8. [8] conductance curve approximation $G(t)$, equivalent normalized sensitivity pulse $s(t)$ and normalized output envelope $p(t)$.

a step-controlled system, during this time period the system behaves as a highly-selective band-pass filter. Slope tuning is included allowing to tune the K_s of the system. This tuning has the undesired effect of reducing $G_{\rm dc}$, thereby reducing the maximum attainable quench frequency for a desired hangover coefficient.

4) Multi Step: The conductance control in [11] is based on a multi-step controlled system. The system's Qs (both during growth and quenching) dictate system 3 dB BW, just as in step-controlled systems. Fig. 9 shows the implemented conductance-controlling function. Both Qs must be as high as possible (low conductance values) to achieve the smallest possible 3 dB BW. These higher Qs come at the expense of lower super regenerative gain and, in most cases, a reduced quench frequency. The work presented in [11] allows for an increase in the maximum quench frequency by adding another level at the beginning of the quench period. This additional high conductance value quickly quenches any oscillation from a previous cycle.

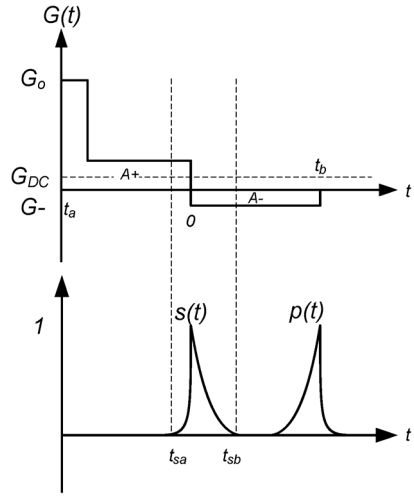

Fig. 9. [11] conductance curve $G(t)$, equivalent normalized sensitivity pulse $s(t)$ and normalized output envelope $p(t)$.

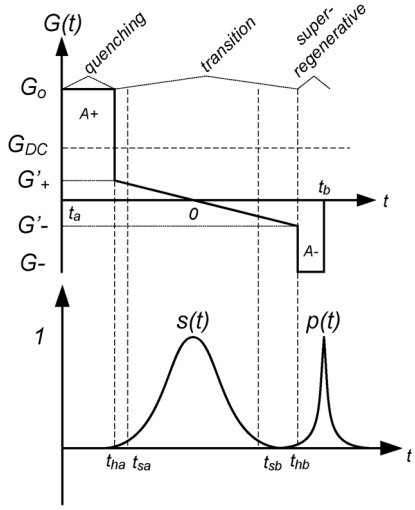

Fig. 10. Proposed optimal conductance signal $G(t)$, equivalent normalized sensitivity pulse $s(t)$, and normalized output envelope $p(t)$.

This action translates to an increase in the system's $G_{\rm dc}$. Inserting a switch parallel to the LC tank implements the high G value.

E. Optimal Quench

The optimal quench signal should allow *independent* control over the system's gain and 3 dB BW, and should allow a high quench frequency. Fig. 10 presents the proposed shape of such a signal which represents a slope-controlled system as long as (7) holds true. There are three distinctive phases in each period. We call these phases quench, transition, and super-regenerative regions. Based on Fig. 10 we define the transition time as a percent of the total quench period or transition time percent $(tt\%)$. This value is

$$tt\% = \frac{(t_{hb} - t_{ha})}{(t_b - t_a)} \times 100\%. \tag{45}$$

The key elements that the designer needs to control are the slope during the transition and the transition time time boundaries (t_{ha}, t_{hb}).

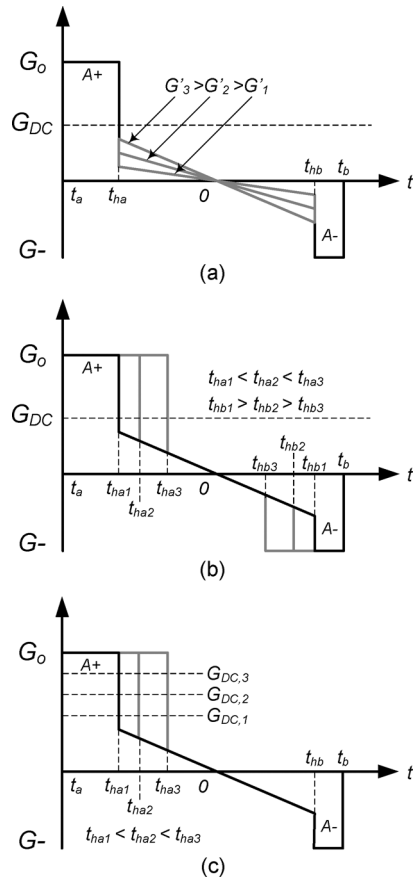

Fig. 11. Quench signal tunning for independent control over: (a) bandwidth; (b) K_s; (c) quench frequency.

1) Optimal Quench Tuning: During the previous discussion the main concern of design has been the 3 dB bandwidth. While this concern is dominant for most narrow band applications, the same would not be so for scenarios where a larger bandwidth is desired, such as ultra-wide band applications [14]. When these scenarios or others are considered classical signals, such as sine wave signals might suffice. Still, the proposed optimal quench signal also provides the needed performance. The ability of the optimal signal to allow *independent* control over bandwidth, gain, and data rate allows for system tuning according to the required needs, setting it apart from other quench signals.

Fig. 11 shows how to tune the optimal signal to obtain the desired parameter tuning with minimal effects on the other parameters, as we shall discuss in further detail in the following paragraphs. The bandwidth can be adjusted by changing the slope of the quench signal during the transition period as shown in Fig. 11(a). The obtained bandwidth

$$BW \propto \sqrt{\frac{|G'|}{C}} \tag{46}$$

where G' is the conductance slope. Keeping t_{ha} and t_{hb} equidistant from $t = 0$ allows the change in slope to maintain the same $G_{\rm dc}$ value and has minimal effects on $(K_s \cdot K_r)$.

The main gain component K_s can be controlled by symmetrically adjusting t_{ha} and t_{hb}, thereby adjusting $tt\%$ as shown in Fig. 11(b). This reduction or increase of $tt\%$ will in turn increase or decrease the area A^-, thus increasing or decreasing K_s as stated by (14). $G_{\rm dc}$ remains constant despite these changes.

Finally, Fig. 11(c) shows that by adjusting t_{ha} the quench signal's dc component is tuned, allowing for different maximum quench frequencies as given by (44).

The synthesis of a piecewise linear quench signal, whether optimal or not, affects the overall receiver's performance. Process variations, device mismatch, and other undesired fabrication effects impact the fidelity of the generated quench signal. Specifically, fluctuation of the values of the desired conductance values create mismatch among the desired gains and hangover coefficient as stated in (14), (42), and (44). Furthermore, these same errors could create frequency-response variation for step-controlled systems as dictated by (34). Meanwhile, errors in the conductance slope G' during the transition time could affect the frequency response of the system for slope controlled systems [cf.(30)]. PVT-mitigating techniques such as constant-g_m biasing may be implemented to alleviate the g_m mismatches. While digitally based tuning schemes may be implemented to lessen the slope divergences. Several previous works have addressed these concerns with of analog [8], [10] and digital [11], [16] solutions.

The thrust of this paper is to determine the optimal quench-signal *shape* and verify with a prototype and laboratory arbitrary-waveform-generator hardware that such a signal indeed provides benefits over conventional and previous shapes. Developing the actual circuitry used to synthesize the desired signal remains an open research problem. For instance, one potential embodiment of the quench signal generator is a direct digital frequency synthesizer (DDFS) connected to a digital-to-analog converter (DAC), which controls the quench signal, similar to that in [8].

IV. Quench Signal Shape Comparison

From the previous discussion, the optimal quench signal (OPT) and the piecewise-linear quench signal both provide the flexibility to control the system's properties. As we shall see, OPT additionally provides *independent* control of system specs and solves the problem of changing hangover coefficient of the piecewise function as the system gain is swept. A theoretical SRO example is now presented to compare the quench signals and their fundamental limitations. Table I describes the specifications of the example system. These values represent a typical system for wireless applications within the ISM band. To achieve these specs, we control the given system with each of the different quench signals. The values in this section are based on the theoretical expressions derived in Section II for a linear-mode system; the next section will compare the expected improvement with measured results.

During the following example we tune several quench signals. Fig. 12 shows how each of the considered quench signals are tuned. The sine, sawtooth, and piecewise linear signals' amplitudes are swept. In contrast, the OPT signal's transition time $(tt\%)$ is swept, as discussed in Section III-E1. Fig. 13 presents the resulting overall $(K_s \cdot K_r)$ gains of several quench signals whose amplitudes have been swept while keeping the

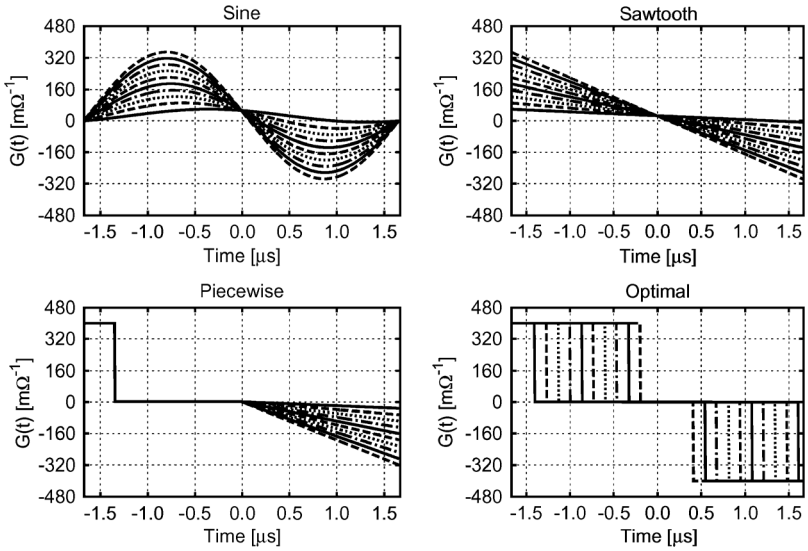

Fig. 12. Different quench signals as their amplitude or $tt\%$ are swept. These waveforms include: sawtooth, sine, optimal, and piecewise linear.

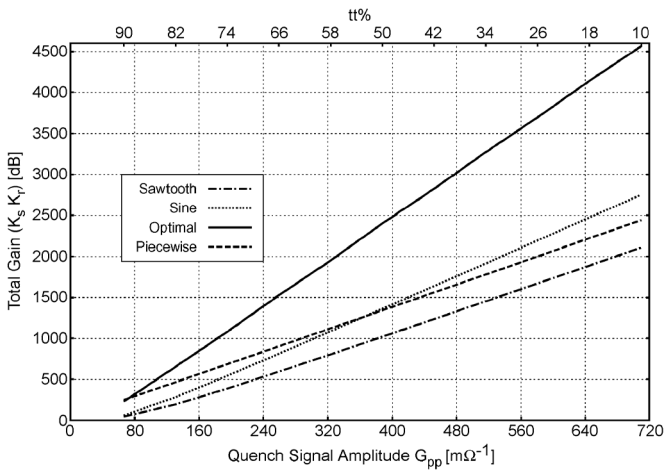

Fig. 13. Gains for different quench signals as their amplitude are swept. These waveforms include sawtooth, sine, optimal, and piecewise linear.

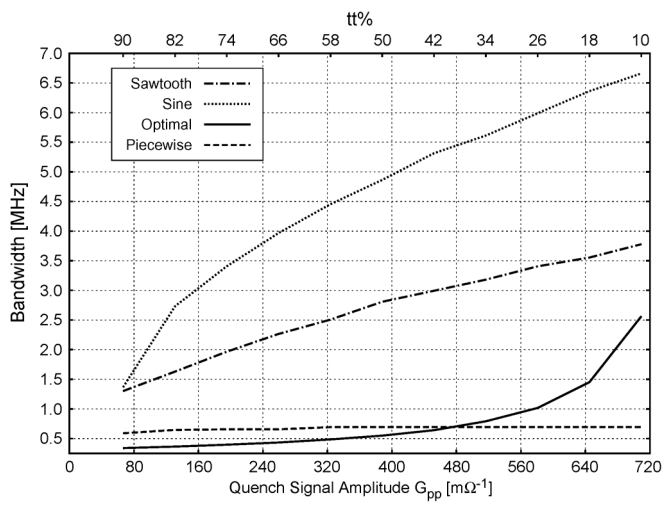

Fig. 14. 3 dB BW for different quench signals as their amplitude are swept. These waveforms include sawtooth, sine, optimal, and piecewise linear.

hangover coefficient at a constant values (except for the piecewise which does not allow a constant hangover coefficient as its amplitude is swept). We plot the curves for example's simplified components and neglect nonidealities which would limit the gain to lower values (≈60 dB, typical) in practice. The displayed trends are nonetheless the same as those for actual systems. Fig. 14 presents the resulting 3 dB bandpass bandwidths for the same set of signals. The main conclusion is that the narrowest 3 dB BW and the largest gain are given by the OPT signal for large $tt\%$. Furthermore, as $tt\%$ decreases, the OPT signal 3 dB BW widens. This widening of the OPT signal 3 dB BW is an effect of OPT signal deviating from the slope-controlled case and resembling a step-controlled system. Meanwhile, the piecewise signal's hangover coefficient drastically increases as the quench-signal amplitude increases. Fig. 15 presents this increase for the previous sweeps. An augmenting hangover coefficient hinders the system performance by lowering the maximum quench frequency as stated in Section III-C.

The main benefit from the piecewise signal is the high-Q filter region, which allows for a widening of the sensitivity pulse, thereby also reducing the 3 dB BW. The same widening of the

TABLE I
SYSTEMS SPECIFICATIONS

Parameter	Value
f_0 [GHz]	2.4
f_q [kHz]	300
K_0 V/V[a]	0.4
Q_0[b]	20
Quench amplitude	$G_{DC} \rightarrow 2(G_0 - G_{DC})$
$tt\%$	10→90

[a] Nominal gain when no feedback is applied (i.e., $1/G_0$).
[b] Quiescent Q for LC tank when no feedback is applied.

sensitivity pulse is achieved with OPT signal. Designing an OPT signal with a slope during the transition period whose min and max values have the same magnitude as the piecewise linear signal's critical conductance achieves the widening of the sensitivity pulse. Finally, tuning $tt\%$ acheives the same or larger gain as the piecewise linear case. Fig. 16 presents the piecewise linear and OPT quench signals waveforms based on the above guidelines on how to obtain the same gain and hangover coefficient. Fig. 17 displays the corresponding frequency response of

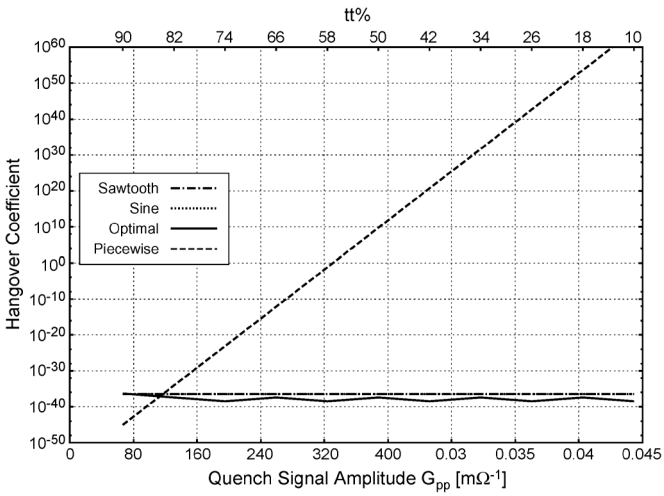

Fig. 15. Hangover coefficient for different quench signals as their amplitude are swept. These waveforms include sawtooth, sine, optimal, and piecewise linear. (N.B.: the sawtooth and sine hangover coefficients overlap each other throughout the entire sweep).

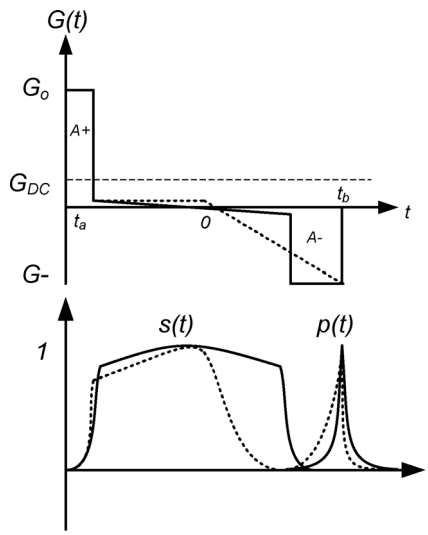

Fig. 16. Quench signals for piecewise linear (dotted line) and OPT (solid line) with identical transition level control during sensitivity period.

these two quench signals given the same overall gain and hangover coefficient. We observe that the OPT quench signal's 3 dB BW (336 kHz) is reduced from the piecewise linear signal's 3 dB BW (651 kHz) by 48.39%.

V. Laboratory Prototype for Proof of Concept

To verify the proposed quench-signal performance and its 3 dB BW reduction, this section discusses a discrete implementation of a super-regenerative oscillator as a proof of concept. The receiver samples the on-off-keyed incoming signal asynchronously. The design example presented operates at 10 MHz, has a quench frequency of 300 Hz, and operates in linear-mode. Fig. 18 presents the schematics of the super-regenerative oscillator (i.e., selective network and positive-feedback amplifier as described in Section II) along with an input buffer.

The presented super-regenerative oscillator is based on a positive feedback oscillator with a frequency-selective network composed of a symmetric dual-T network. The oscillator, although not an explicit negative resistance with a resonant

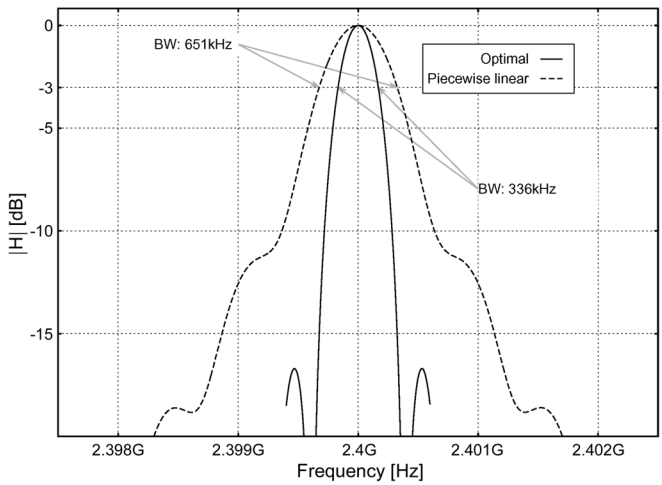

Fig. 17. Frequency response of OPT and piecewise linear signals for the same gain and hangover coefficient.

tank, can be mapped to such an LC network. Fig. 19 subdivides both oscillators—the conceptual LC oscillator employed in our theoretical derivation and the positive feedback oscillator used in experimental verification—into the principal blocks of an SRO, namely the incoming signal, frequency selective network, and positive feedback network.

For the feedback oscillator case, drawing an analogy to root loci, we can view the system's characteristic equation as a two-pole response with "parameter" K_a, respectively the amount of positive feedback

$$\left(\frac{s}{\omega_o}\right)^2 + \frac{s}{\omega_o}\left(\frac{1}{Q_o} - K_a\right) + 1 = 0 \tag{47}$$

where ω_o is the natural frequency, Q_o is the quiescent Q (for $K_a = 0$), and K_a is the feedback amplifier gain (assumed constant for simplicity). Sufficiently increasing K_a produces RHP poles, inducing oscillations startup. Table II summarizes the correspondence of both systems.

The main concern for SRO design is the control of the startup characteristics of the system. Given the startup characteristics of the designed SRO resemble those of a resonant network, all the presented discussion holds true.

The loaded network presents a quiescent Q of 2.4 and a loop gain of -7 dB. The variable gain amplifier AD83330 [28] adds the remaining phase shift to achieve the necessary 360° and its gains controls the overall loop gain. The AD8330's gain is controlled by an external signal provided by an arbitrary waveform generator through the control signal V_{MAG} (while V_{DBS} provides a static gain [28]). This generated signal controls the system feedback signal, which can be shown (see [21] for details) to be equivalent to controlling the SRO quench signal, and therefore all the systems properties, namely its gain, data rate, and 3 dB BW. The input buffer is implemented by the fully differential amplifier THS4503 [29] feedback amplifier. This amplifier provides a unity gain to the incoming signal.

For a fair comparison of the systems' 3 dB BWs, all signals were adjusted to attain the same overall gain and a sufficiently small hangover coefficient. Fig. 20 presents the implemented quench signals. These signals include classical sine and sawtooth shapes, as well as the piecewise linear and the OPT signal.

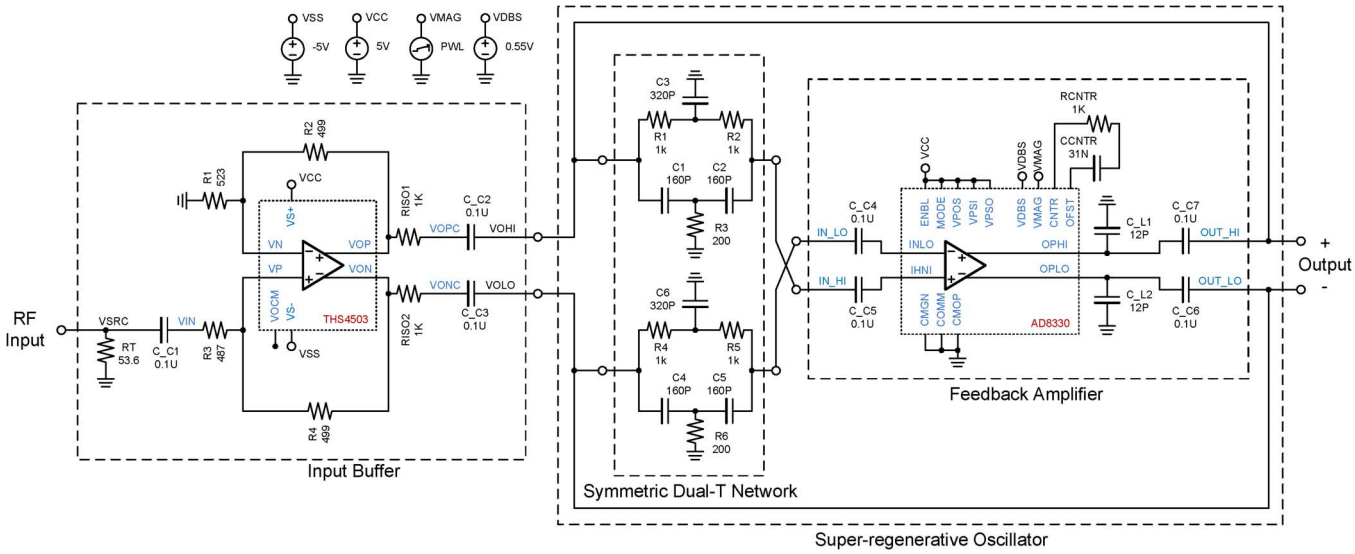

Fig. 18. Schematic of the implemented super-regenerative oscillator with input buffer.

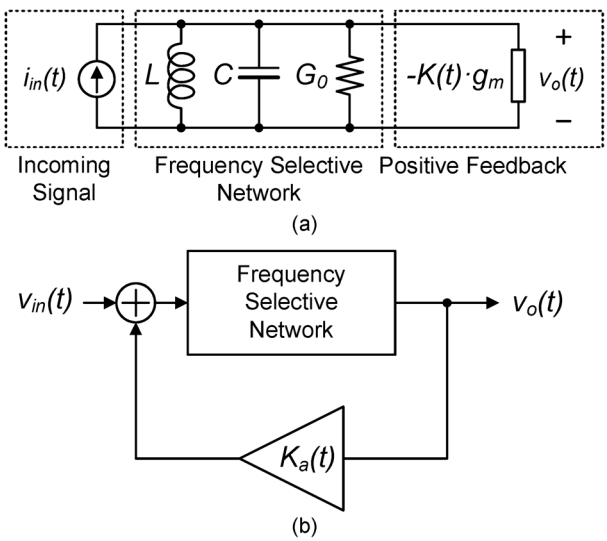

Fig. 19. Main SRO conceptual blocks for: (a) LC tank network; (b) positive feedback oscillator.

TABLE II
CORRESPONDENCE BETWEEN LC TANK AND POSITIVE FEEDBACK IMPLEMENTATIONS OF SROS

Parameter	LC Tank	Positive Feedback
Input signal	$i_{in}(t)$	$v_{in}(t)$
Output signal	$v_o(t)$	$v_o(t)$
Quiescent Q	$\sqrt{\frac{C}{L}}\frac{1}{G_o}$	Q_o
Natural frequency	$1/\sqrt{LC}$	ω_o
Negative g_m	$K(t)g_m$	$K_a(t)$

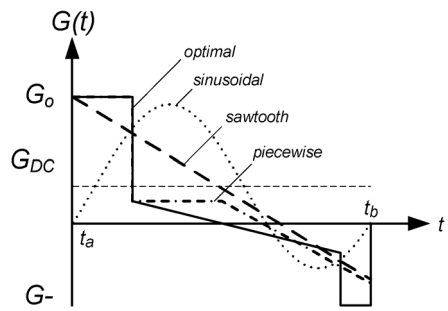

Fig. 20. Quench signals in the proof of concept example: sinusoidal (dotted), sawtooth (dashed), piecewise linear (dashed-dotted) and optimal (solid).

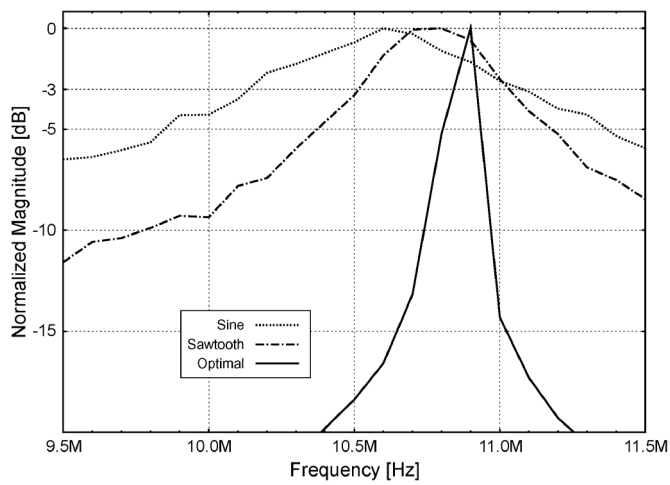

Fig. 21. Frequency response for different quench signals: sinusoidal (dotted), sawtooth (dot-dashed), and optimal (solid).

Fig. 21, 22 show the measured frequency-response curves to determine the 3 dB BW for these quench signals. We obtain these curves by plotting the normalized output-voltage-envelope peak value vs. the swept input frequency. Clearly, the OPT signal provides the smallest 3 dB BW of all. Reshaping of the quench signal from the piecewise linear to the OPT shape reduces the 3 dB BW by 42.83%.

Note that the laboratory specs have a different frequency than those discussed in Table I. We chose a lower frequency design for our laboratory prototype to minimize parasitic effects, allowing a more controlled experiment of the quench signal performance.

Our use of a lower oscillation frequency is justified: 1) because the gain and hangover coefficient are independent of frequency of oscillation as long as the conductance and capacitor $(G(t)/C)$ is scaled (i.e., we deal with the *normalized* waveform shape), and 2) because we examine bandwidth normalized to the frequency of oscillation. Therefore, scaling and normalizing as

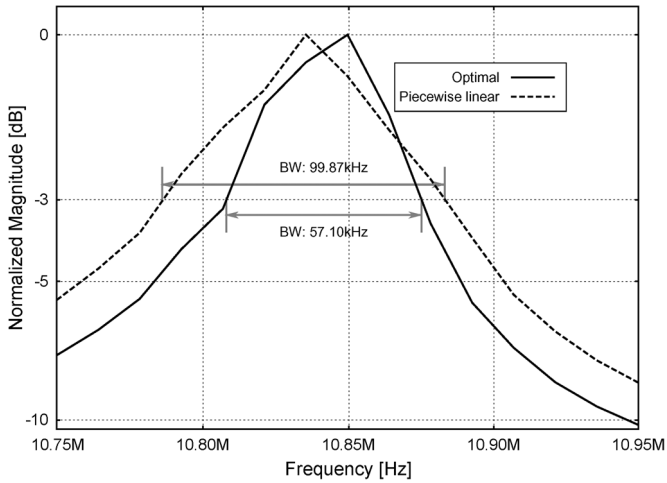

Fig. 22. Frequency response for optimal (solid) and piecewise linear (dashed) quench signals.

described above permits reduction of the oscillation frequency for a more straightforward lab measurement. The quench-waveform shapes' normalized performances are independent of the implemented system as long as: a) the designed SRO's startup characteristic resembles those of a resonant network, and b) the tuning guidelines presented in Section III-E1 are followed.

VI. Conclusion

We have proposed an optimal quench signal for super-regenerative receivers and experimentally demonstrated its superior 3 dB BW performance and independent design control over SRR specifications compared to other recently published quench signals. Furthermore, this paper has shown that the main concern when designing a super-regenerative receiver should be the quench signal's shape. The receiver's frequency response, gain, and the maximum data rate are all tightly related to this shape. The slope of the waveform during the transition between stable and oscillating system controls the frequency response. The quench signal's average value controls the maximum quench frequency, which in turn limits the system's maximum data rate. The super-regenerative gain, which typically governs the overall receiver gain, depends exponentially on the area under the quench signal during the oscillating phase. The proposed quench-signal shape yields the smallest 3 dB BW, and unlike previously proposed works, allows independent control of key receiver parameters gain, frequency response, and quench frequency. Finally, we implemented a proof-of-concept design, whose measured results confirm the theoretical discussion. The implemented system outperforms all classical wave shapes and decreases the 3 dB BW by more then 42.83% from that of conventional systems' quench signals.

Acknowledgment

The authors would like to thank Mr. Alfredo Costilla-Reyes for his help in the design and measurements of the proof-of-concept hardware.

References

[1] E. H. Armstrong, "Wireless Receiving System," U.S. Patent 1 113 149, Oct. 6, 1914.

[2] E. H. Armstrong, "Some recent developments of regenerative circuits," *Proc. Inst. Radio Eng.*, vol. 10, no. 4, pp. 244–260, Aug. 1922.

[3] E. H. Armstrong, "Method of Receiving High-Frequency Oscillations," U.S. Patent 1 342 885, Jun. 8, 1920.

[4] P. Favre, N. Joehl, A. Vouilloz, P. Deval, C. Dehollain, and M. J. Declercq, "A 2-V 600- μA 1-GHz BiCMOS super-regenerative receiver for ISM applications," *IEEE J. Solid-State Circuits*, vol. 33, no. 12, pp. 2186–2196, Dec. 1998.

[5] A. Vouilloz, M. Declercq, and C. Dehollain, "A low-power CMOS superregenerative receiver at 1 GHz," *IEEE J. Solid-State Circuits*, vol. 36, no. 3, pp. 440–451, Mar. 2001.

[6] N. Joehl, C. Dehollain, P. Favre, P. Deval, and M. Declerq, "A low-power 1-GHz super-regenerative transceiver with time-shared PLL control," *IEEE J. Solid-State Circuits*, vol. 36, no. 7, pp. 1025–1031, Jul. 2001.

[7] B. Otis, Y. H. Chee, and J. Rabaey, "A 400 μW – RX, 1.6 mW-TX super-regenerative transceiver for wireless sensor networks," in *Proc. IEEE Int. Solid-State Circuits Conf. (ISSCC)*, Feb. 2005, vol. 1, pp. 396–606.

[8] J.-Y. Chen, M. P. Flynn, and J. P. Hayes, "A fully integrated auto-calibrated super-regenerative receiver in 0.13- μm CMOS," *IEEE J. Solid-State Circuits*, vol. 42, no. 9, pp. 1976–1985, Sep. 2007.

[9] F. X. Moncunill-Geniz, P. Pala-Schonwalder, C. Dehollain, N. Joehl, and M. Declercq, "An 11-Mb/s 2.1-mW synchronous superregenerative receiver at 2.4 GHz," *IEEE Trans. Microw. Theory Tech.*, vol. 55, no. 6, pp. 1355–1362, Jun. 2007.

[10] J. L. Bohorquez, J. L. Dawson, and A. P. Chandrakasan, "A 350 μW CMOS MSK transmitter and 400 μW OOK super-regenerative receiver for medical implant communications," in *Proc. IEEE Symp. VLSI Circuits*, Jun. 2008, pp. 32–33.

[11] J. Ayers, K. Mayaram, and T. S. Fiez, "An ultralow-power receiver for wireless sensor networks," *IEEE J. Solid-State Circuits*, vol. 45, no. 9, pp. 1759–1769, Sep. 2010.

[12] N. B. Buchanan, V. F. Fusco, and J. A. C. Stewart, "A 7.5-GHz super regenerative detector," *IEEE Trans. Microw. Theory Tech.*, vol. 50, no. 9, pp. 2198–2202, Sep. 2002.

[13] P. E. Thoppay, C. Dehollain, and M. J. Declercq, "A 7.5 mA 500 MHz UWB receiver based on super-regenerative principle," in *Proc. 34th Eur. Solid-State Circuits Conf. (ESSCIRC)*, Sep. 2008, pp. 382–385.

[14] M. Pelissier, D. Morche, and P. Vincent, "Super-regenerative architecture for UWB pulse detection: From theory to RF front-end design," *IEEE Trans. Circuits Syst. I, Reg. Papers*, vol. 56, no. 7, pp. 1500–1512, Jul. 2009.

[15] Y. H. Liu and T. H. Lin, "A delta-sigma pulse-width digitization technique for super-regenerative receivers," *IEEE J. Solid-State Circuits*, vol. 45, no. 10, pp. 2066–2079, Oct. 2010.

[16] M. Vidojkovic, P. X. H. Harpe, S. Rampu, K. C. Z. L. H. Imamura, B. Busze, F. Bouwens, M. Konijnenburg, J. Santana, A. Breeschoten, J. Huisken, G. Dolmans, and H. de Groot, "A 2.4 GHz ULP OOK singlechip transceiver for healthcare applications," in *Proc. IEEE Int. Solid-State Circuits Conf. (ISSCC)*, Feb. 2011, pp. 458–460.

[17] M. Arlelid, L. E. Wernersson, M. Egard, and E. Lind, "A 60 GHz superregenerative oscillator for implementation in an impulse radio receiver," in *Proc. IEEE Int. Conf. Ultra-Wideband (ICUWB)*, Sep. 2010, vol. 1, pp. 1–4.

[18] J. R. Whitehead, *Super-Regenerative Receivers*. Cambridge, U.K: Cambridge Univ. Press, 1950.

[19] D. G. Tucker, "The history of positive feedback: The oscillating audion, the regenerative receiver, and other applications up to around 1923," *Radio Electron. Eng.*, vol. 42, no. 2, pp. 69–80, Feb. 1972.

[20] A. Vouilloz, M. Declercq, and C. Dehollain, "Selectivity and sensitivity performances of superregenerative receivers," in *Proc. 1998 IEEE Int. Symp. Circuits Syst. (ISCAS)*, May 1998, vol. 4, pp. 325–328.

[21] F. X. Moncunill-Geniz, P. Pala-Schonwalder, and O. Mas-Casals, "A generic approach to the theory of superregenerative reception," *IEEE Trans. Circuits Syst. I, Reg. Papers*, vol. 52, no. 1, pp. 54–70, Jan. 2005.

[22] P. E. Thoppay, C. Dehollain, and M. J. Declercq, "Noise analysis in super-regenerative receiver systems," in *Proc. Ph.D. Res. Microelectron. Electron. (PRIME)*, Apr. 2008, pp. 189–192.

[23] J. L. Bohorquez, A. P. Chandrakasan, and J. L. Dawson, "Frequency-domain analysis of super-regenerative amplifiers," *IEEE Trans. Microw. Theory Tech.*, vol. 57, no. 12, pp. 2882–2894, Dec. 2009.

[24] A. D. Polyanin and V. F. Zaitsev, *Handbook of Exact Solutions for Ordinary Differential Equations*. Boca Raton, FL: Chapman & Hall/CRC, 2003.

[25] I. M. Gottlieb, *Practical Oscillator Handbook*. Oxford, U.K.: Newnes, 1997.

[26] W. Edson, "Noise in oscillators," *Proc. IRE*, vol. 48, no. 8, pp. 1454–1466, Aug. 1960.
[27] R. G. Lyons, *Understanding Digital Signal Processing*. Upper Saddle River, NJ: Prentice-Hall, 2010.
[28] "AD8330: Low cost DC to 150 MHz variable gain amplifier," Analog Devices, 2010 [Online]. Available: http://www.analog.com/en/specialty-amplifiers/differential-amplifiers/ad8330/products/product.html
[29] "THS4503: Wideband, low-distortion fully differential amplifier," Texas Instruments, 2003 [Online]. Available: http://www.ti.com/lit/ds/symlink/ths4503.pdf

Félix Omar Fernández-Rodríguez (S'03) was born in Rio Piedras, Puerto Rico. He received the B.S. and M.S. degrees in electrical engineering from the University of Puerto Rico, Mayaguez Campus, in 2000 and 2003, respectively. He is currently working toward the Ph.D. degree at the Analog and Mixed Signal Center, Texas A&M University, College Station.

In the summer and fall of 2000, he was an Analog IC Design Engineer (Co-op) with Texas Instruments, Dallas, TX, where he designed a macro model for switched capacitor low power Sigma Delta ADC for mobile applications. In summer 2004, he was Analog IC Design Engineer (Co-op) with Texas Instrument, Dallas, where has was part of the design team of the Mixed Signal Power and Control unit. His research interests include low power RF receivers and built in testing for RF circuits.

Edgar Sánchez-Sinencio (S'72–M'74–SM'83–F'92–LF'10) was born in Mexico City, Mexico. He received the degree in communications and electronic engineering (professional degree) from the National Polytechnic Institute of Mexico, Mexico City, the M.S.E.E. degree from Stanford University, Stanford, CA, and the Ph.D. degree from the University of Illinois at Champaign-Urbana, in 1966, 1970, and 1973, respectively.

He is currently the TI J. Kilby Chair Professor and Director of the Analog and Mixed-Signal Center, Texas A&M University, College Station. His research work has more than 2930 citations according to the Thomson Reuters Scientific Citation Index. He has graduated 42 M.Sc. and 37 Ph.D. students. He is a coauthor of six books on different topics, such as RF circuits, low-voltage low-power analog circuits, and neural networks. His present interests are in the area of power management, RF-communication circuits, analog and medical electronics circuit design.

Dr. Sánchez-Sinencio is a former Editor-in-Chief of IEEE TRANSACTIONS ON CIRCUITS AND SYSTEMS II. In November 1995 he was awarded a Honoris Causa Doctorate by the National Institute for Astrophysics, Optics and Electronics, Mexico. This degree was the first honorary degree awarded for microelectronic circuit design contributions. He is a corecipient of the 1995 Guillemin-Cauer Award for his work on cellular networks. He was also the corecipient of the 1997 Darlington Award for his work on high-frequency filters. He received the IEEE Circuits and Systems Society Golden Jubilee Medal in 1999. He also received the prestigious IEEE Circuits and Systems Society 2008 Technical Achievement Award. His Web site can be found at http://amesp02.tamu.edu/\simsanchez/.